Distance-Informed Neural Eikonal Solver for Reactive Dynamic User-Equilibrium of Macroscopic Continuum Traffic Flow Model

Yun Ye, *Member, IEEE*, Haoyang Liang, *Member, IEEE*, Jian Sun, *Member, IEEE*, and Xiqun Chen

***Abstract*— This paper revisits the Reactive Dynamic User-Equilibrium (RDUE) model for dynamic traffic assignment (DTA) of macroscopic traffic flow in two-dimensional continuum space, focusing on the Eikonal equation—a crucial partial differential equation (PDE) with specific boundary conditions. Traditionally, solving Eikonal equations has relied on iterative numerical methods through the discretization of the continuum space. However, this discretization compromises the precision of numerical solutions and could lead to non-convergence issues during iterative processes. This study refers to Physics-Informed Neural Networks (PINNs) and develops the Distance-Informed Neural Eikonal Solver (NES-DI) for solving Reactive Dynamic User-Equilibrium models. While the previously proposed Neural Eikonal Solver (NES) performs badly in a strong heterogeneous cost field with large cost differences, NES-DI explicitly considers the influence of solid boundaries during the factorization process by incorporating accurate distance information. Numerical examples of RDUE at both the static and dynamic levels are presented to illustrate the performance and applications of the NES-DI framework. The results demonstrate that NES-DI greatly outperforms both NES and the fast sweeping method. Moreover, NES-DI overcomes the limitations of discretization, enabling predictions of solutions at arbitrary locations within the computational domain. At the dynamic level, transfer learning is employed to leverage historical solutions to solve RDUE problems more efficiently. Overall, NES-DI shows the potential of solving reactive dynamic problems with strong heterogeneity, which offers a promising alternative to discretization-reliant numerical methods.**

Received 16 April 2024; revised 21 October 2024; accepted 16 February 2025. Date of publication 4 March 2025; date of current version 2 June 2025. This work was supported in part by Zhejiang Provincial Natural Science Foundation of China under Grant LQN25E080011; in part by Ningbo Natural Science Foundation under Grant 2024J440; in part by the National "111" Centre on Safety and Intelligent Operation of Sea Bridges under Grant D21013; and in part by the National Natural Science Foundation of China under Grant 52302378, Grant 72171210, Grant 72350710798, and Grant 72431009. The work of Haoyang Liang was supported by Shanghai Super Post-Doctoral Incentive Program. The Associate Editor for this article was A. Hegyi. *(Corresponding author: Xiqun Chen.)*

Yun Ye is with the Faculty of Maritime and Transportation, Ningbo University, Ningbo 315211, China, also with the Collaborative Innovation Center of Modern Urban Traffic Technologies, Southeast University, Nanjing 211189, China, and also with the National Traffic Management Engineering & Technology Research Center, Ningbo University Sub-Center, Ningbo 315832, China (e-mail: yeyun1@nbu.edu.cn).

Haoyang Liang and Jian Sun are with the College of Transportation Engineering and the Key Laboratory of Road and Traffic Engineering, Ministry of Education, Tongji University, Shanghai 201804, China (e-mail: lianghy@connect.hku.hk; sunjian@tongji.edu.cn).

Xiqun Chen is with the Institute of Intelligent Transportation Systems, College of Civil Engineering and Architecture, Zhejiang University, Hangzhou 310058, China, and also with Zhejiang Provincial Engineering Research Center for Intelligent Transportation, Hangzhou 310058, China (e-mail: chenxiqun@zju.edu.cn).

Digital Object Identifier 10.1109/TITS.2025.3543972

***Index Terms*— Macroscopic continuum traffic flow, reactive dynamic user-equilibrium, physics-informed neural networks, Eikonal equation, dynamic traffic assignment.**

I. Introduction

DYNAMIC traffic assignment (DTA) based on continuum-space models has been a potent and effective tool for understanding and managing multidimensional traffic systems, particularly in addressing travel choice problems within dense urban networks [1], [2], [3], [4] and within crowd dynamics [5], [6], [7]. In these continuum modeling approaches, the road network is conceptualized as a two-dimensional (2D) continuum space, while the traffic states, indicated by macroscopic variables, are predicted by solving sets of partial differential equations (PDEs). This macroscopic continuum approach avoids prohibitive computation burden and complex parameter sets in the link–level DTA models [3]. Within this framework, one of the commonly-used assumptions is that travelers with heterogeneous preferences are assumed to follow a reactive user-optimal strategy: They reactively choose the walking directions along the routes with the lowest costs determined by the instantaneous traffic conditions at any given moment. This assumption enables the system to attain a continuum equilibrium state amidst the dynamic evolution of traffic, which forms the Reactive Dynamic User-Equilibrium (RDUE) model [5], [8], [9].

Despite its effectiveness, RDUE models face significant challenges, primarily their reliance on numerical solvers [10], [11]. Typically, the set of PDEs in every RDUE model comprises a continuum equation, represented by a set of Euler equations, and a route strategy equation, represented by an Eikonal equation. Eikonal equation is a nonlinear first-order PDE that is encountered in problems of wave propagation, widely used in many applications, such as geometric optics [12], image processing [13], computer vision [14], and others [15]. Traditional numerical methods have been developed to approximate the physical-relevant solution. The most commonly used methods include the Fast Sweeping Method (FSM) [16] or Fast Marching Method (FMM) [17]. Since Eikonal equations describe the propagation of a front or wavefront in a given medium, FMM develops an entropy-satisfying upwind scheme for gradient approximations with a fast sorting mechanism to solve the discretized PDE,

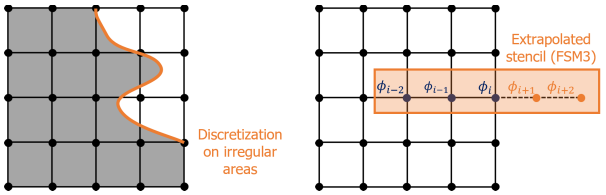

(a) Discretization problem (b) Ghost-point problem

Fig. 1. Challenges associated with the traditional numerical methods.

while FSM updates the wavefront in a direction-independent manner during the Gauss-Seidel iterations. The dependence on these iteration-based numerical methods affects RDUE's computational efficiency and necessitates the convergence of numerical solutions obtained through FSM and FMM.

While FMM and FSM have been useful in solving many various RDUE problems, they encounter significant challenges in meeting the precision and efficiency requirements when addressing complex scenarios. First, the precision of the solution obtained via the methods hinges on the maximum cell size post-discretization within the computational domain [18], [19]. Given that a DTA problem typically occurs within a 2D continuum-space characterized by irregular physical boundaries (see Fig. 1a), achieving convergent solutions near these boundaries necessitates exceptionally fine meshing. This requirement precipitates a substantial surge in the computational cost, as the complexity of these methods does not fall below $O(N)$, where N represents the number of grid points. Second, employing high-order finite difference schemes introduces additional complexities, as depicted in Fig. 1b. The extrapolation of the ghost-points in the wide stencil will also dampen the accuracy of solutions and even hinder convergence [20]. Apart from the challenges, the computational efficiency of the methods has considerable potential for enhancement in the dynamic continuum problems. Usually, the initial solution value at each time step that needs to be updated during the iterations is set significantly high, despite the minimal variance observed between successive time steps during dynamic evolutions [1], [7]. In other words, the numerical methods cannot efficiently relay information from one time step to the next, undermining their efficacy in resolving dynamic problems.

In response to these challenges, this study introduces the application of Physics-Informed Neural Networks (PINNs) [21], which is a recent advancement in deep learning and scientific computing that combines the strengths of neural networks and PDEs to solve complex physical problems. In PINNs, PDEs are embedded into the loss function of PINNs using automatic differentiation, so that physics information can be considered in the neural network training process. This framework has been successfully integrated with integer-order PDEs, integer-differential equations, fractional PDEs, or stochastic PDEs [22]. For instance, many studies have used PINNs to solve PDEs like Navier-Stocks equation, Burger's equation, Poisson equation, etc. [23], [24], [25]. Specifically, studies have also been conducted to solve Eikonal equation using PINNs [26], [27], [28]. Among these works, the Neural Eikonal Solver (NES) proposed in [28] shows the best performance in both accuracy and efficiency. Although the existing NES performs well in many homogeneous and heterogeneous cases, the performance is unsatisfying when facing a strong heterogeneous cost field, which is a common situation for the RDUE problem because of complex geometries consisting of travelers, wall boundaries, and obstacles. Hence, this issue must be addressed when developing PINNs-based methods for solving Eikonal equations in 2D macroscopic traffic flow studies.

In this paper, we propose a novel Distance-Informed Neural Eikonal Sover (NES-DI) for solving Eikonal equation of the RDUE problem with a strong heterogeneous cost field. The factorized Eikonal equation is introduced to account for strong heterogeneity, and the Distance-Informed (DI) module is proposed to estimate the distance distribution by numerical methods according to geometry settings. NES-DI takes advantage of PINNs and numerical methods, achieving better performance in RDUE problems than existing methods. Besides, transfer learning based on NES-DI is also proposed to solve the RDUE problem at the dynamic level. The main contributions of this study are listed as follows:

1) Due to the absence of explicit labels within the training dataset for the resolution of PDEs, traditional deep neural networks exhibit limitations in learning the underlying relationships and dynamics of the equations. This research is among the first batch of studies to leverage PINNs for solving PDEs in 2D macroscopic traffic flow analyses, thereby providing a viable framework for related studies and illuminating the potential of PINNs for solving traffic models with PDEs.
2) The proposed NES-DI method utilizes the factorization form of the distance function equation, and successfully separates the distance information component from the neural network fitting component, thereby well integrating numerical methods and PINNs. The numerical methods address complex geometry settings and provide distance information, upon which PINNs enhance the performance. This strategy capitalizes on the strengths of numerical methods and PINNs, circumventing the ghost-point issues associated with higher-order finite difference methods and providing an efficient solution to RDUE problems.
3) A transfer learning technique is proposed to solve the RDUE problem at the dynamic level, which enables the information of the previous time step to be utilized in the current time step to improve efficiency while maintaining accuracy.

The paper is organized as follows. Section II reviews recent studies related to macroscopic continuum traffic flow models and PINNs-based methods in transportation research field. Section III further introduces the preliminaries of Eikonal equation and the RDUE model. Section IV proposes the PINNs-based method for solving the RDUE problem, i.e., NES-DI. Section V tests the performance of the proposed NES-DI method for different cost fields and compares it with the numerical method and traditional NES. In Section VI,

we provide a discussion of NES-DI, including its advantages, limitations, and future studies. Section VII concludes the paper.

II. Literature Review

A. Macroscopic Continuum Traffic Flow Model

Currently, there are two types of traffic flow models, i.e. microscopic models, and macroscopic models. Microscopic models, including car-following model [29], [30] and cellular automata model [31], [32], are capable of detailing the behavior of each vehicle, such as speed, acceleration, and position, as well as the interactions between vehicles and their surrounding environment, but necessitate significant computational and storage resources. Conversely, macroscopic models may never achieve the same level of descriptive accuracy, but are able to capture the macroscopic characteristics of traffic flow (i,e., density, flow, and speed) by regarding traffic flow as a type of flow based on the continuum assumption. Furthermore, according to different abstraction forms of traffic networks, macroscopic models can be divided into discrete model and continuum model. Discrete model considers traffic networks as composed of discrete road segments and describes each segment individually. On the other hand, continuum model focus on the macroscopic characteristics of traffic flow within the network. It assumes that the network is dense enough to be regarded as a 2D continuous space, where travelers can choose to travel in any direction. Within this framework, traffic parameters such as demand, cost, and flow can be represented by smooth mathematical functions [33], [34].

Macroscopic continuum traffic flow models have many advantages, including reduced problem size, less data required, and a more realistic representation of the system and spatially varying macroscopic characteristics of the traffic network [8]. Thus, it is particularly suitable for densely populated urban areas with high road densities, and has been widely used in DTA problems. For example, Tao et al. [35] introduced a system-optimal model, where users select routes that minimize the total cost for the entire traffic system. Du et al. [1] developed a predictive dynamic user-optimal model for monocentric cities, assuming that travelers are fully aware of future traffic conditions, and select routes that minimize the predicted actual total travel cost. Building on this, Du et al. [36] extended it to the case of anisotropic conditions in multiple Central Business Districts (CBDs). In contrast to the predictive user equilibrium model, the RDUE model describes travelers' movement based on the assumption that the predictive information is not available when making route choices, thus users would choose routes that minimize the instantaneous total travel cost based on current traffic information. Hughes [5] proposed a continuum theory for pedestrian flow, which derived the equations of motion governing the two-dimensional pedestrian flow. Based on this, Huang et al. [10] found that pedestrian route choice strategy in Hughes' model satisfies the RDUE principle. In this model, the pedestrian demand is time varying, and the pedestrian density, flux, and walking speed are governed by the conservation equation. Jiang et al. [37] further extended the RDUE model for multi-center cities.

TABLE I
Recent PINNs-Based Studies in Transportation Research Field

Year	Author	Research topic
2020	Huang and Agarwal	Traffic state estimation
2021	Shi et al.	Traffic state estimation
2021	Shi et al.	Traffic state and fundamental diagram estimation
2021	Mo et al.	Car-following models
2022	Huang et al.	Traffic state estimation
2023	Geng et al.	Vehicle trajectory prediction
2023	Liu et al.	Car-following models
2023	Lu et al.	Traffic state and queue profile estimation
2024	Zhang et al.	Traffic state estimation
2024	Zhao et al.	Traffic state estimation

In addition, the solving methods of macroscopic continuum models have also been studied. Hughes [38] systematically proposed the framework of a 2D continuum pedestrian flow model but did not provide numerical solution methods for the model. Huang et al. [10] introduced the reactive dynamic user-optimal conditions for continuum pedestrian flow models, specifically focusing on the problem of unidirectional pedestrian flow, which for the first time developed a higher-order numerical method for solving continuum pedestrian flow models. Subsequently, Huang et al. [39] proposed a model for bidirectional pedestrian flow. Xia et al. [19] solved the reactive unidirectional pedestrian flow model using the discontinuous finite element method based on an unstructured grid (triangular grid). Jiang et al. [40] used a triangular grid to solve the reactive bidirectional pedestrian flow model. Jiang et al. [2] modeled and numerically simulated reactive and predictive high-order pedestrian flow models, and detailed the similarities and differences between the two models.

To conclude, most previous studies used numerical methods to solve macroscopic continuum traffic flow models, which suffer from discretization problem [18], [19], ghost-point problem [20], and dynamic solving efficiency problem [1], [7]. To address these challenges, PINNs-based method is proposed to solve the RDUE problem of macroscopic continuum traffic flow models.

B. PINNs-Based Studies in Transportation Research Field

PINNs represent a computational approach that integrates deep learning with principles of physics. The core idea of PINNs is to incorporate the terms derived from physical laws into the loss function of the neural network, ensuring that the network adheres to physical laws while learning from data. Currently, in the field of transportation studies, PINNs have been successfully applied to traffic state estimation [41], [42], [43], [44], [45], [46], [47], car-following model [48], [49], vehicle trajectory prediction [50], etc. Related studies are summarized in Table I. In these contexts, PINNs tend to focus more on using the physical laws of transportation fields to guide the learning process of the network, which helps improve the accuracy of algorithms, especially in situations where data might be scarce or incomplete.

Besides, PINNs are also widely used in scientific computing that combines the strengths of neural networks and PDEs to solve complex physical problems [21], [22], [23], [24], [25], [26], [27], [28]. Among these, PINNs method have also been proposed to solve Eikonal equation [26], [27], [28], and NES is the current state-of-art algorithm which shows superior performance than other methods [28]. However, this paradigm is rarely found in transportation studies. When PINNs are utilized for solving PDEs, they primarily leverage the physical information of PDEs. By incorporating the constraints of PDEs as part of the loss function, PINNs can learn solutions that satisfy these constraints. This method does not require the mesh generation typical of traditional numerical methods but instead directly seeks an approximate representation of the solution through optimization. This is particularly useful in handling complex geometries or high-dimensional problems.

Different from previous PINNs-based studies in the field of transportation research, this study represents the first endeavor of introducing PINNs to solve PDEs in 2D continuum macroscopic traffic flow models, specifically Eikonal equation pertinent to the RDUE problem. This investigation delineates several distinctions from previous PINNs-based paradigms, such as traffic state estimation. First, in terms of objectives, the goal in solving PDEs is to find analytical or approximate solutions that satisfy specific physical constraints, while in applications such as traffic state estimation, the objective is to predict future traffic conditions based on existing data and physical laws. Moreover, when solving PDEs in this study, PINNs rely more on the form of PDEs and boundary conditions, whereas in traffic state estimation, PINNs need to combine actual traffic data with physical laws for learning.

III. Preliminaries

A. Static Eikonal Equation

Eikonal equation is a first-order nonlinear PDE and has been applied in many science and engineering problems as a high-frequency approximation to the propagation of waves in heterogeneous media. It can be expressed as

$$\|\bigtriangledown_r \phi(\mathbf{x}_r)\| = C(\mathbf{x}_r), \mathbf{x}_r \in \Omega, \tag{1a}$$

$$\phi(\mathbf{x}_s) = 0, \tag{1b}$$

where $\|\cdot\|$ is the Euclidean norm, $\phi(\mathbf{x}_r)$ represents the cost potential to any given receiver point $\mathbf{x}_r$ originating from the source point $\mathbf{x}_s$, $\bigtriangledown_r$ denotes the spatial differential operator, $C(\mathbf{x}_r)$ is the cost defined on Ω, and Ω is the domain in $\mathbb{R}^d$ with d as the dimension of space. Eikonal equation describes the first-arrival travel time for a fixed source point $\mathbf{x}_s$, constrained by the boundary condition $\phi(\mathbf{x}_s) = 0$. Eikonal equation implies that the gradient of the first-arrival time surface is inversely proportional to the velocity of the wavefront propagation. Notably, in the field of transportation, the term "receiver" $\mathbf{x}_r$ represents the individuals' positions at a specific time, and "source" $\mathbf{x}_s$ represents the destination of individuals. This is common in traffic scenarios, such as pedestrian evacuations, where there are often only one or a few destinations but many individuals' positions all over the space.

It is challenging to derive the analytical solution to Eikonal equation. Therefore, numerical methods, such as FSM and FMM, have been proposed to solve this problem based on the discretized form of a uniform rectangular mesh:

$$\hat{H}((\phi_x)^-_{i,j}, (\phi_x)^+_{i,j}; (\phi_y)^-_{i,j}, (\phi_y)^+_{i,j}) = C(\mathbf{x}_r), \tag{2}$$

where $\hat{H}$ is the Godunov type monotone Hamiltonian, $(\phi_x)^\pm_{i,j}, (\phi_y)^\pm_{i,j}$ are the numerical approximations of the left and right derivatives, $i = 1, 2, \ldots, N_x$ and $j = 1, 2, \ldots, N_y$ indicate the number of the node on the uniform rectangular mesh. This study applies the Godunov fast-sweeping method [16] to derive the ground truth solution for the Eikonal equation.

B. Reactive Dynamic User-Equilibrium Model

In the static part of RDUE problems, travelers are generally assumed to make route choices based on the instantaneous information of the two-dimensional (2D) geometry Ω, formulating an Eikonal equation with similar mathematical descriptions. Refer to Hughes' continuum model [5], a cost potential field, denoted as $\phi(x, y)$, is denoted as the potential distribution of the walking cost estimated from the instantaneous information. Travelers tend to walk along the direction which minimizes the cost potential, thus the relationship between the expected moving direction $\vec{v}$ and the cost potential field ϕ is then derived as

$$\vec{v}(x, y) = -\frac{\nabla\phi(x, y)}{\|\nabla\phi(x, y)\|}, (x, y) \in \Omega. \tag{3}$$

Let $C(x, y)$ denote the local travel cost and Γ_D is the destination in the geometry where $\phi = 0$, a static potential field model that describes the aggregative relationship between the potential field and local cost can be given as the following Eikonal equation:

$$\|\nabla\phi(x, y)\| = C(x, y), \ (x, y) \in \Omega, \tag{4a}$$

$$\phi(x, y) = 0, \ (x, y) \in \Gamma_D. \tag{4b}$$

Eq. (3) and Eq. (4) describe the path-choice behavior of travelers who walk along a path with the lowest instantaneous cost. To solve the DTA problems, the previous static potential field model is usually associated with the continuum theory to formulate the final PDE set (Eq. (5)) of RDUE at the dynamic level. This commonly-used model assumes travelers reactively choose the move direction based on the distribution of global instantaneous travel cost $\phi(x, y, t)$. Though many high-order continuum models have been developed recently to capture more complex traffic characters [7], [9], the static part relies on similar Eikonal solvers. Therefore, this study focuses on the basic form of the RDUE model as follows:

$$\begin{cases} \rho_t + (\rho u)_x + (\rho v)_y = 0 \\ ||\nabla\phi(x, y, t)|| = C(x, y, t) \\ |\boldsymbol{v}| = V(\rho), \boldsymbol{v}(x, y, t)// - \nabla\phi(x, y, t) \\ \text{initial conditions at } t = 0; \text{ boundary conditions,} \end{cases} \tag{5}$$

where ρ_t indicates the derivative of density ρ with respect to time t, $\boldsymbol{v} = (u, v)$ indicates the speed along dimensions x and y. In the first equation, the net flow of pedestrians

into a field, denoted as $-\nabla \cdot \mathbf{f} = -((\rho u)_x + (\rho v)_y)$, equals the rate of accumulation of pedestrians in the field, denoted as ρ_t. The second equation models the reactive user-optimal route strategy through the static Eikonal equation at each time step t, $V(\rho)$ in the third equation assumes the fundamental diagram relationship between velocity and density, and the speed direction is parallel to the negative gradient of cost potential ϕ. Given initial values and boundary settings, the RDUE model formulates a set of PDEs with appropriate initial and boundary conditions, which can be solved by the traditional numerical methods, such as the Lax-Friedriches scheme and FSM.

IV. Physics-Informed Neural Networks

This study develops the modified NES, a PINNs-based method, to solve the static Eikonal equations in transportation studies. The general solution procedure consists of the following steps:

- *Step 1.* Transform Eikonal equation into factorized Eikonal equation;
- *Step 2.* Determine the distance distribution using FSM or FMM;
- *Step 3.* Build fully connected neural networks for the prediction of factorized solutions;
- *Step 4.* Set a proper loss function, which includes the Hamiltonian form of Eikonal equation;
- *Step 5.* Train the neural network with the weights initialized by Kaiming initialization [51] until the error estimation reaches expectation.

A. NES for Factorized Eikonal Equation

To avoid singularity at the source location, an improved factorized form of Eq. (4) is introduced as follows:

$$\phi_{\boldsymbol{\theta}}(\mathbf{x}_r) = R \cdot \bar{\sigma}\left(F_{\boldsymbol{\theta}}(\mathbf{x}_r)\right), \tag{6}$$

where R is the distance from the receiver location $\mathbf{x}_r = (x_r, y_r)$ to the source location $\mathbf{x}_s = (x_s, y_s)$ considering the geometry settings, which will be introduced later; F_θ is the output of neural-network with parameters θ; $\bar{\sigma}(x)$ is a bounding function introduced by [28] that can improve the efficiency in approximating the solution in Eq. (6), see Eq. (7) as follows:

$$\bar{\sigma}(x) = (C_{max} - C_{min}) \frac{1}{1 + e^{-x}} + C_{min}, \tag{7}$$

where C_{max} and C_{min} denote the maximum and minimum values of the considered cost field respectively, so that $\bar{\sigma}(x)$ is constrained by $[C_{min}, C_{max}]$.

Eikonal equations are usually applied to traffic problems in complex geometries, which include walls, obstacles, and blocks. To consider this geometry heterogeneity in Eikonal equation, researchers either assigned a fixed large potential [5] $\phi(x, y) = \phi_{max}$ or assigned a large local cost [52] $C(x, y) = C_{max}$ for those points in the boundaries, i.e. $(x, y) \in \Gamma_H$. This study applies the latter method, which forms a continuous distribution of the solutions.

B. Distance-Informed Approach

So far, the PINNs-based Eikonal solvers [26], [27], [28] applied the Euclidean distance in the calculation of R, i.e. $R = \|\mathbf{x}_r - \mathbf{x}_s\|$. This simple assumption enables a simple form of the loss function in PINNs but shifts the burden of geometry heterogeneity to the training of neural networks. Consequently, the prediction results inside and around the boundary are not satisfying, especially for the heterogeneous cost field with large cost differences.

To address this problem of strong heterogeneity, a PINNs-based framework incorporated with numerical methods is proposed, i.e., NES-DI. Unlike traditional NES, NES-DI employed numerical methods to provide distance information, which greatly relieves the burden of neural networks in handling a strong heterogeneous cost field. Only the first-order FSM or FMM is used due to its high efficiency and ability to avoid ghost-point issues. Specifically, for given cost $\mathbf{C}^{m\times n}$, the first-order FSM or FMM is first used to calculate the distance matrix $\mathbf{R}^{M\times N}$, where $m \times n$ refers to the mesh size, and $M \times N$ equals $m \times n$ here if the output of FSM or FMM is directly used as distance matrix. After getting the distance matrix through FSM or FMM, it is further interpolated into a continuous surface using TensorFlow, i.e., $R_\beta(\mathbf{x}_r)$, which allows for the backward propagation of gradients. Based on the distance information, neural networks can fully leverage its capabilities to provide accurate travel time predictions at any location within the computational domain. In addition, we propose a two-step interpolation method, i.e., Distance-Informed Neural Eikonal Solver with Interpolation (NES-DI(I)), which introduces the modified Akima piecewise cubic Hermite interpolation (MAKIMA) method [53], a much more powerful interpolation method than linear interpolation, to first densify the distance matrix obtained from numerical methods and provide more accurate distance information. Therefore, in the NES-DI(I), the size of distance matrix, i.e., $M \times N$, is larger than $m \times n$.

The factorized Eikonal equation of NES-DI is given as Eq. (8). Unlike NES, as distance R is no longer the Euclidean distance of source-receiver points, the neural network output is no longer bounded by minimum and maximum costs.

$$\phi_{\boldsymbol{\theta},\boldsymbol{\beta}}(\mathbf{x}_r) = R_\beta(\mathbf{x}_r) \cdot F_{\boldsymbol{\theta}}(\mathbf{x}_r), \tag{8}$$

where $R_\beta(\mathbf{x}_r)$ represents the output of the function that maps from receiver points $\mathbf{x}_r$ to distance, i.e., $R_\beta(\mathbf{x}_r) : \mathbb{R}^2 \to \mathbb{R}^1$, and β denotes the parameters of the mapping function; $F_\theta(\mathbf{x}_r)$ is the output of the artificial neural networks and θ represents the corresponding parameters, which will be explained in Section IV-D.

C. Loss Function

The loss function for the factorized Eikonal equation is defined as

$$L(\boldsymbol{\theta}, \boldsymbol{\beta}, p) = \frac{1}{N_r} \sum_{\mathbf{x}_r} |\mathcal{H}_p(\mathbf{x}_r, \phi_{\boldsymbol{\theta},\boldsymbol{\beta}})|, \tag{9}$$

where N_r is the number of receivers, and Hamiltonian $\mathcal{H}_p$ is defined as

$$\mathcal{H}_p(\mathbf{x}_r, \phi_{\boldsymbol{\theta},\boldsymbol{\beta}}) = \frac{1}{p}\left[\frac{\|\nabla\phi_{\boldsymbol{\theta},\boldsymbol{\beta}}(\mathbf{x}_r)\|^p}{C(\mathbf{x}_r)^p} - 1\right]. \tag{10}$$

In this loss function, p is the hyper-parameter, and the choice of p will significantly influence the attention of the training process and thus contribute to the training efficiency. If $p > 1$, the significance of high-cost errors will be increased, particularly in the obstacle area, and thus the singularities can be better approximated here. On the contrary, if $p < 1$, the significance of low-cost errors will be increased, thus singularities are more likely to be approximated in the low-cost area [28]. In NES-DI, p is taken as 0.2 to consider the importance of singularities in the low-cost area for problems with strong heterogeneity.

D. Algorithm Architecture

To solve RDUE problems both at static and dynamic levels, this study proposes a dual-level algorithmic architecture, comprising NES-DI and NES-DI-transfer. The implementation of these architectures is elucidated as follows.

1) Static Level: Based on the NES training architecture, the proposed NES-DI is presented in Fig. 2.

The inputs are the given receiver points $\mathbf{x}_r = (x_r, y_r)$, followed by a scaling process $1/\max|\mathbf{x}_r|$. Rescaling primarily impacts the parameters within the neural networks, and has been demonstrated effective in NES [28]. On the other hand, the given receiver points are utilized as the input for the DI module.

NES utilizes a fully connected neural network (FCNN), a universal approximator representing the mapping $F_\theta(x) : \mathbb{R}^n \to \mathbb{R}^m$, to extract information from inputs and to serve as a factorized part. FCNN with $K-1$ hidden layers can be expressed as Eq. (11).

$$h_k = g_k\left(\Theta_k h_{k-1} + b_k\right), k = 0, \ldots, K, \tag{11}$$

where $h_k \in \mathbb{R}^{N_k \times 1}$ is the hidden state of layer k with N_k units, $\Theta_k \in \mathbb{R}^{N_k \times N_{k-1}}$ are the kernel weights to be learned, b_k is the bias weight, and g_k is the activation function to produce non-linearity. In this study, Gaussian function $g_k(x) = e^{-x^2}$ is used as it has a natural extremum resembling the singularity shape and is infinitely differentiable, which has proven to outperform $relu$, $atan$, and elu [28]. The network training is based on gradient descent, and the Adam optimization method is applied due to its fast and accurate convergence for most problems [54]. In this study, the FCNN has 4 hidden layers with 100 units.

The DI module is introduced to provide accurate distance information for the factorized Eikonal equation. Details have been illustrated in Section III-B.

2) Dynamic Level: Transfer learning is introduced to solve the RDUE problem in the continuum framework. The following transfer framework is proposed to use prior information from the previous time step and transfer the knowledge to the current time step to improve efficiency while ensuring accuracy. Specifically, distance matrix R of the current time step is given by the prediction of a well-trained neural network from the previous time step, so that FSM or FMM is not needed for every time step. The transfer framework is shown in Fig. 3. The procedure consists of the following steps:

- *Step 1.* Using NES-DI to solve the RDUE problem in the initial time step, where numerical methods are required to provide initial distance information;
- *Step 2.* The distance matrix of the current time step is predicted by well-trained neural networks of the previous time step;
- *Step 3.* Using NES-DI-transfer to solve the RDUE problem of the current step based on the distance information given by the previous step;
- *Step 4.* After several time steps, re-calibrate the distance matrix by numerical methods to eliminate the accumulated errors.

V. Numerical Examples

The relative mean absolute error (RMAE) is introduced in this study to evaluate the performance of PINNs as follows:

$$\text{RMAE} = \frac{\sum_{\mathbf{x}_r}|\phi_{ref} - \phi_{\theta,\beta}|}{\sum_{\mathbf{x}_r}|\phi_{ref}|}, \tag{12}$$

where ϕ_{ref} denotes the ground truth solution, and $\phi_{\theta,\beta}$ denotes the predicted solution of PINNs.

Three numerical examples are designed and tested in this section. The first is Eikonal equation with explicit solutions, the second is a static model of routing strategy in vehicular traffic, and the third is a dynamic model of routing strategy in pedestrian evacuation. In cases of example 2 and example 3, where analytical solutions of the Eikonal equations are unavailable, numerical solutions derived from the first-order FSM [16] with a relatively large mesh size are considered as the ground truth solution. All numerical examples were performed on the GPU NVIDIA RTX A5000 (24GB GDDR6).

A. Example 1: Trigonometric Eikonal Equation (Static)

In the numerical examples, this study first applies NES-DI to address a conventional two-dimensional problem, specifically, trigonometric Eikonal equation. This kind of Eikonal equation, known for the smoothness of its analytical solution, has been commonly used to evaluate the precision of numerical methods [16]. In this example, the cost function is given as

$$C(x,y) = \begin{cases} \frac{\pi}{2}\sqrt{\sin^2(\pi + \frac{\pi}{2}x) + \sin^2(\pi + \frac{\pi}{2}y)}, \\ \qquad (x,y) \notin \Gamma_H, \\ 2\pi\sqrt{\sin^2(\pi + \frac{\pi}{2}x) + \sin^2(\pi + \frac{\pi}{2}y)}, \\ \qquad (x,y) \in \Gamma_H, \end{cases} \tag{13}$$

and the destination (source point) is $\Gamma_D : (0,0)$. The whole computational domain is $\Omega : [-1,1] \times [-1,1]$, where the wall is located at $\Gamma_H : (x,y)$ s.t. $\cos\left(\pi + \frac{\pi}{2}x\right) + \cos\left(\pi + \frac{\pi}{2}y\right) \geq -1.5$. The exact solution for this problem

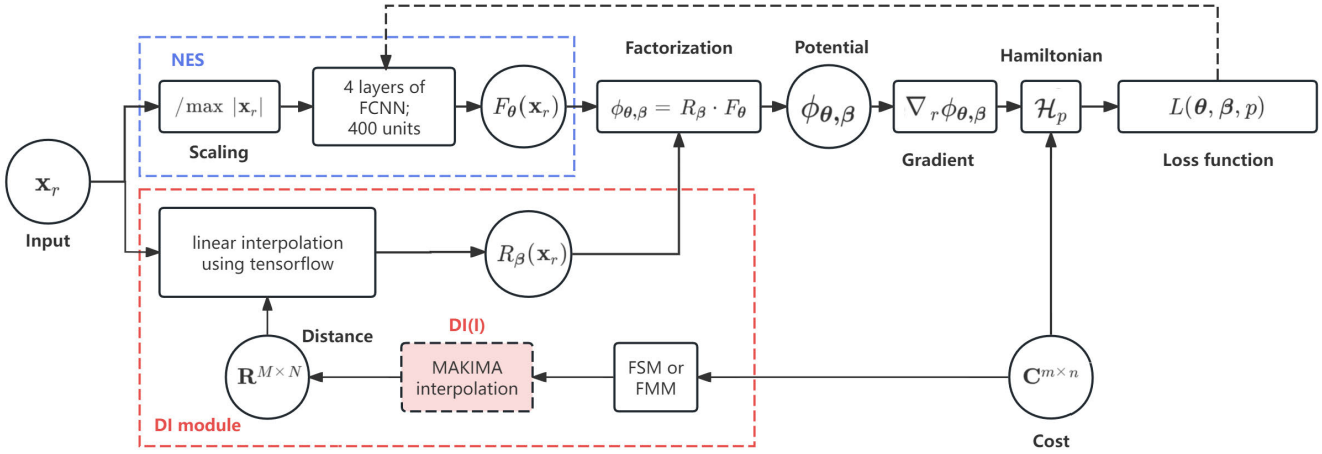

Fig. 2. Flow diagram of NES-DI architecture.

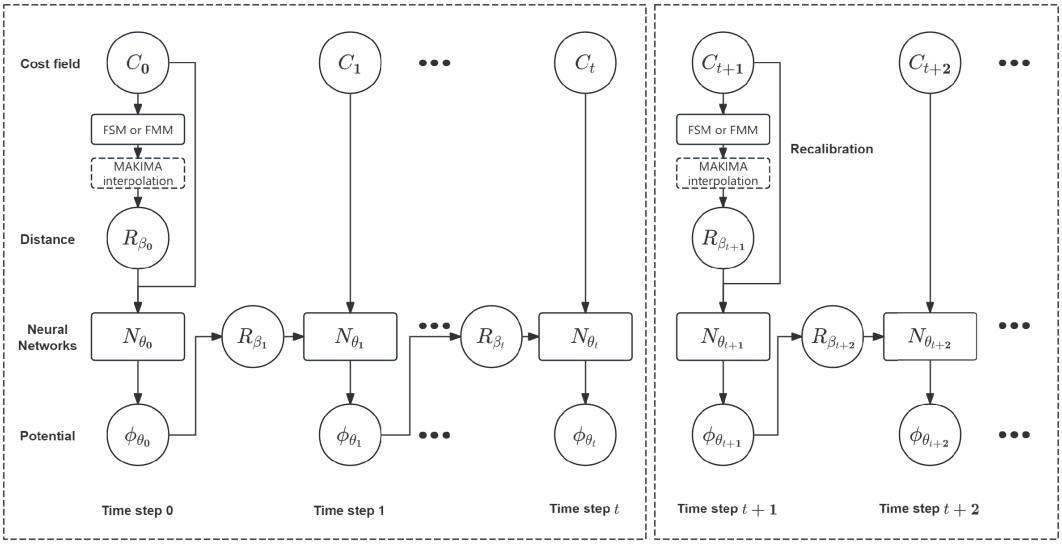

Fig. 3. Transfer learning framework with NES-DI for solving RDUE problems at the dynamic level.

is

$$\phi(x, y) = \begin{cases} \cos\left(\pi + \dfrac{\pi}{2}x\right) + \cos\left(\pi + \dfrac{\pi}{2}y\right) + 2, \\ \qquad (x, y) \notin \Gamma_H, \\ 4\cos\left(\pi + \dfrac{\pi}{2}x\right) + 4\cos\left(\pi + \dfrac{\pi}{2}y\right) + 1 \\ \qquad (x, y) \in \Gamma_H. \end{cases} \tag{14}$$

Four solvers (i.e., first-order FSM, NES, NES-DI, NES-DI(I)) are tested and compared with different mesh sizes. The predicted solution contours of potential distributions are presented in Fig. 4, the distribution of relative absolute error (RAE) is presented in Fig. 5, and the detailed RMAE and training time of four solvers are compared in Table II.

Apart from the RMAE values calculated for the entire region, this study also evaluates the RMAE in free areas for all numerical examples. This is because RDUE problems commonly focus on the solutions in obstacle-free areas. The results show that the potential in regions with obstacles is typically different from that in free regions due to the assignment of different cost distributions.

Based on the results in Table II, the performance of FSM is unsatisfactory on sparse meshes. However, as the grid is refined, its accuracy improves and eventually surpasses that of NES. Fig. 6 illustrates the performance of FSM across different mesh sizes, showing that with a sufficiently fine grid, the FSM solution closely approximates the true analytical solution. As such, numerical solutions on refined meshes are often used as the ground truth in problems where an analytical solution is unavailable, as applied in previous PINNs-related studies [28], [55].

As the cost field changes smoothly within the whole area, which exhibits relatively weak heterogeneity, the performance of NES is acceptable for the whole computational domain. Nonetheless, the efficacy of NES diminishes significantly within free areas, though the accuracy in this region is of primary importance in practical applications. In contrast, both NES-DI and NES-DI(I) demonstrate robust performance not only across the entire computational domain but also within

TABLE II
PERFORMANCE COMPARISON OF IMPROVED NES-BASED METHODS IN EXAMPLE 1

Solver	Mesh size	RMAE of all (x, y) (%)	RMAE of $(x, y) \notin \Gamma_H$ (%)	Training time (s) / Epoch number
FSM	41×41	6.56	12.35	–
FSM	101×101	3.02	4.99	–
FSM	201×201	1.50	2.50	–
FSM	401×401	0.73	1.25	–
FSM	1001×1001	0.29	0.50	–
NES	41×41	**1.62**	3.22	102.81/3000
NES	101×101	**0.56**	2.56	103.37/3000
NES	201×201	0.60	2.99	97.68/3000
NES	401×401	0.40	2.19	173.96/3000
NES	1001×1001	0.58	2.86	697.25/3000
NES-DI	41×41	2.64	5.27	14.10/200
NES-DI	101×101	1.29	2.29	14.35/200
NES-DI	201×201	0.61	0.97	14.50/200
NES-DI	401×401	0.30	0.49	18.81/200
NES-DI	1001×1001	**0.08**	**0.11**	62.35/200
NES-DI(I)	41×41	2.60	**2.99**	16.69/200
NES-DI(I)	101×101	1.24	**0.86**	14.67/200
NES-DI(I)	201×201	**0.54**	**0.39**	14.67/200
NES-DI(I)	401×401	**0.26**	**0.21**	19.24/200
NES-DI(I)	1001×1001	0.12	0.21	62.77/200

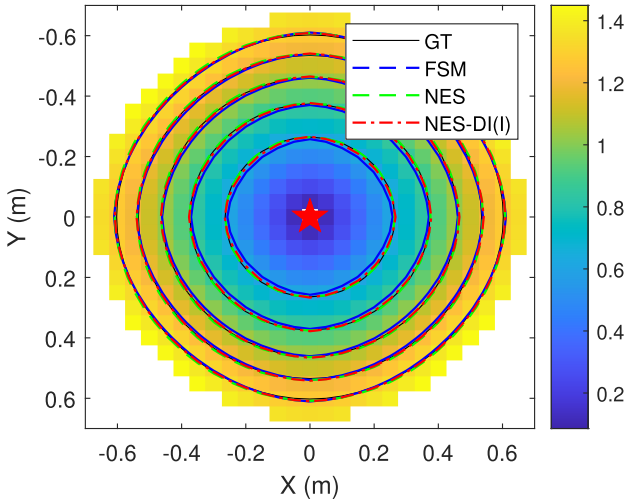

Fig. 4. Contours of the potential distribution predicted using analytical solution (GT), FSM, NES, and NES-DI(I) in the free area under the mesh size of 41×41 for example 1. The white area represents the wall. The heatmap shows the cost magnitude in the free area.

free areas, with NES-DI(I) exhibiting superior efficacy in free areas across a majority of mesh sizes. Specifically, under the mesh size of 1001×1001, NES-DI achieves a substantial reduction in RMAE, exceeding 62% for all (x, y) and 78% for $(x, y) \notin \Gamma_H$, when compared to FSM. Moreover, relative to NES, the reduction in RMAE exceeds 86% for all (x, y) in the computation domain and 96% for $(x, y) \notin \Gamma_H$. Furthermore, integrating FSM within NES-DI and NES-DI(I) to provide accurate distance information significantly enhances efficiency, enabling convergence to an optimal solution within approximately 200 epochs. This represents a substantial reduction in training time, approximately 90%, when compared to the NES approach.

From Fig. 5, it can be intuitively observed that FSM and NES present large RAE near the source point, which reflects their limited efficacy in addressing singularities around the source point in the heterogeneous cost field. As the mesh size increases, there is a significant improvement in the performance of FSM; however, the performance of NES continues to be unsatisfying. Conversely, the solving methods proposed in this study, namely NES-DI and NES-DI(I), consistently demonstrate robust performance across all mesh densities. This suggests that NES-DI and NES-DI(I) possess superior capabilities in managing the challenges posed by singularities in heterogeneous cost fields, underscoring their potential applicability in various computational scenarios.

B. Example 2: Modeling of Cost Potential in Urban Cities (Static)

In example 2, the static Eikonal equation from the RDUE problem, which models route choices in urban areas [1], is examined. For this static scenario, random density values are generated at grid points, and a thin-plate spline fit function is used to represent the density distribution across the computational domain. The solution involves calculating the potential distribution by solving the 2D Eikonal equation based on the instantaneous total cost. Additionally, two destinations are considered in this case to showcase the capability of NES-DI in handling multiple-source-point problems.

The whole computational domain is $\Omega : [0, 50]$ km $\times [0, 50]$ km and the two source points are located at $\Gamma_D : (16, 16)$ and $(36, 36)$. The obstacles include three lakes, which are located at $\Gamma_H : [4, 12]$ km $\times [4, 16]$ km, $[20, 35]$ km $\times [10, 16]$ km, $[18, 28]$ km $\times [32, 42]$ km, and a river, which is located at $\Gamma_H : [0, 18] \cup [20, 50]$ km $\times [28, 30]$ km.

The cost function is given by

$$C(x, y) = \begin{cases} \kappa \left(\dfrac{1}{U_m(1 + \gamma d)e^{-\beta\rho^2}} + 10^{-8}\rho^2 \right), \\ \qquad (x, y) \notin \Gamma_H, \\ 100, \qquad (x, y) \in \Gamma_H, \end{cases} \tag{15}$$

where $\beta = 2 \times 10^{-6}$ km^4/veh^2, $\gamma = 4 \times 10^{-3}$ km^{-1}, $U_m = 56$ km/h, $\kappa =$ \$90 /h; $\rho(x, y)$ and

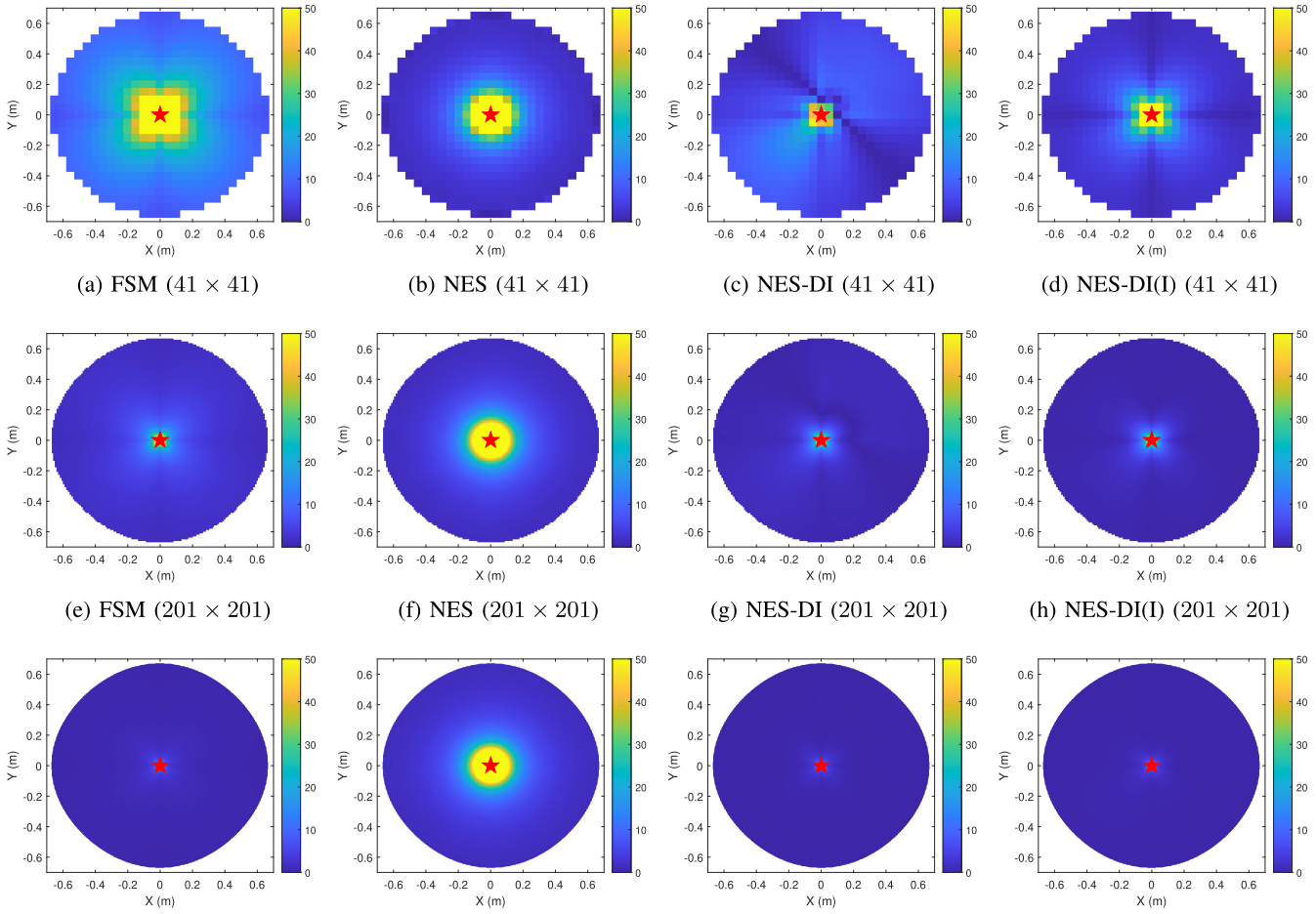

(a) FSM (41 × 41) (b) NES (41 × 41) (c) NES-DI (41 × 41) (d) NES-DI(I) (41 × 41)

(e) FSM (201 × 201) (f) NES (201 × 201) (g) NES-DI (201 × 201) (h) NES-DI(I) (201 × 201)

(i) FSM (1001 × 1001) (j) NES (1001 × 1001) (k) NES-DI (1001 × 1001) (l) NES-DI(I) (1001 × 1001)

Fig. 5. Distribution of RAE in the free area derived from the four methods under different mesh sizes for example 1. The white area indicates the wall. The red star indicates the source point.

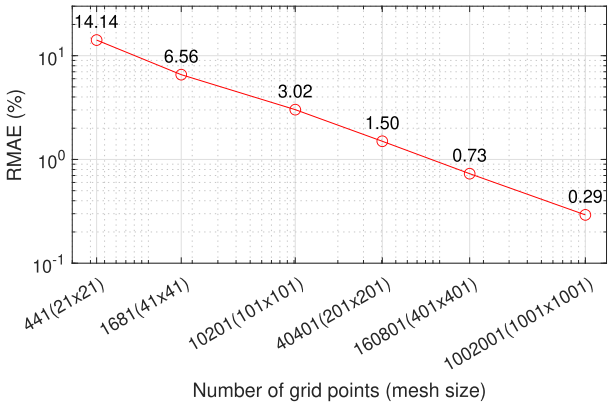

Fig. 6. RMAE of FSM under different mesh sizes in example 1.

$d(x, y) = \|(x, y) - (x_s, y_s)\|$ indicates the density distribution and Euclidean distance between one of the source location $(x_{s,1}, y_{s,1}) = (16, 16)$ and location (x, y), respectively. The density distribution is randomly generated in this example.

Four solvers (i.e., first-order FSM, NES, NES-DI, NES-DI(I)) are tested and compared with different mesh sizes. Owing to the absence of an exact analytical solution for the scenario under consideration, this study designates the solution derived from FSM under the mesh size of 10001 × 10001 as the ground truth solution. The predicted solution contours of the potential distribution are presented in Fig. 7, and the detailed RMAE and training time are compared in Table III.

In Fig. 7, NES shows unsatisfying performance in such problems with strong heterogeneity, constrained by its simplified Euclidean distance information. Based on the detailed performance comparison presented in Table III, both NES-DI and NES-DI(I) show promising performance in the whole computational domain and free areas. Specifically, under the mesh size of 51 × 51, NES-DI achieves a reduction in RMAE exceeding 51% for $(x, y) \notin \Gamma_H$ relative to FSM. In comparison to NES, NES-DI achieves remarkable RMAE reductions exceeding 91% for all (x, y) and 85% for $(x, y) \notin \Gamma_H$, which underscores the profound impact of the DI module in enhancing the performance of NES. The integration of MAKIMA interpolation within the DI module, as implemented in NES-DI(I), precipitates further performance enhancements. Under most mesh sizes, NES-DI(I) accomplishes an RMAE reduction when benchmarked against NES-DI. However, the superiority of NES-DI and NES-DI(I) varies slightly under different mesh sizes, possibly due to the interpolation error

TABLE III
PERFORMANCE COMPARISON OF IMPROVED NES-BASED METHODS IN EXAMPLE 2

Solver	Mesh size	RMAE of all (x, y) (%)	RMAE of $(x, y) \notin \Gamma_H$ (%)	Training time (s) / Epoch number
FSM	51×51	2.97	3.08	–
FSM	101×101	1.69	2.04	–
FSM	201×201	0.84	1.10	–
FSM	501×501	0.49	0.65	–
FSM	1001×1001	0.27	0.36	–
NES	51×51	30.38	10.44	500.40/3000
NES	101×101	31.25	11.56	469.80/3000
NES	201×201	32.09	12.78	921.00/3000
NES	501×501	31.26	13.18	2487.00/3000
NES	1001×1001	30.90	12.43	11263.20/3000
NES-DI	51×51	2.64	**1.50**	11.92/200
NES-DI	101×101	1.29	1.20	11.38/200
NES-DI	201×201	0.62	0.74	14.70/200
NES-DI	501×501	0.36	0.43	29.26/200
NES-DI	1001×1001	0.19	0.21	91.71/200
NES-DI(I)	51×51	**2.53**	1.55	12.62/200
NES-DI(I)	101×101	**1.29**	**1.11**	12.06/200
NES-DI(I)	201×201	**0.60**	**0.61**	14.90/200
NES-DI(I)	501×501	**0.34**	**0.41**	29.42/200
NES-DI(I)	1001×1001	**0.18**	**0.20**	91.54/200

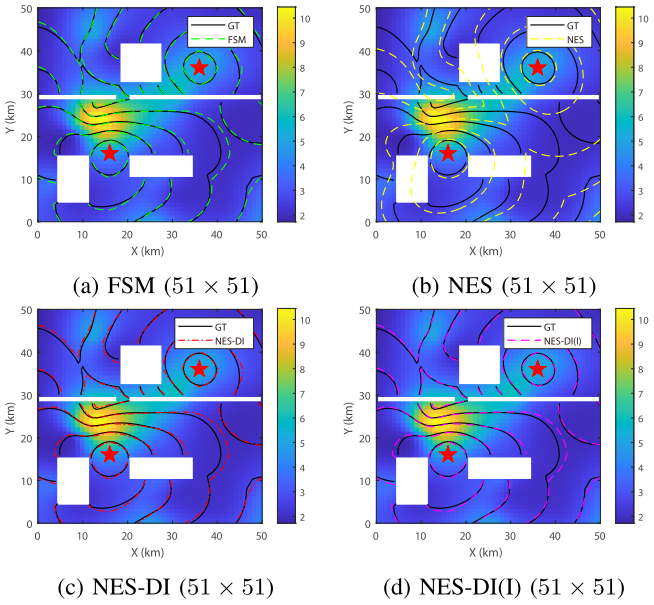

(a) FSM (51×51) (b) NES (51×51)

(c) NES-DI (51×51) (d) NES-DI(I) (51×51)

Fig. 7. Contours of the potential distribution predicted using FSM, NES, NES-DI, and NES-DI(I) in the free area compared to ground truth solution (GT) for example 2. The heatmaps show the cost magnitude in the free area.

of MAKIMA. Overall, this empirical evidence attests to the effectiveness of both NES-DI and NES-DI(I) in addressing computational challenges in heterogeneous cost fields.

Moreover, the performance of FSM, NES-DI, and NES-DI(I) in this case improves significantly with denser mesh sizes. Conversely, the performance of NES fails to exhibit significant enhancement in response to the augmentation of the dataset size. Specifically, under the mesh size of 1001×1001, NES-DI achieves a pronounced reduction in RMAE exceeding 29% for all (x, y) and 41% for $(x, y) \notin \Gamma_H$ when compared to FSM. Furthermore, when compared to NES, NES-DI achieves a substantial RMAE reduction exceeding 99% for all (x, y) and 98% for $(x, y) \notin \Gamma_H$. Such findings indicate the superior performance of NES-DI under denser mesh configurations.

Additionally, under these conditions of increased grid density on the computation domain, the performance metrics of NES-DI and NES-DI(I) begin to converge, suggesting a diminishing return on the improvements offered by NES-DI(I) under denser mesh sizes. Regarding the computational training duration, similar to the results in example 1, both NES-DI and NES-DI(I) achieve significant reduction in training time compared to NES, e.g., over 99% reduction in training time under the mesh size of 1001×1001.

C. Example 3: RDUE for Pedestrian Dynamics (Dynamic)

In example 3, the RDUE problem that dynamically predicts route choices under scenarios of obstructed evacuation has been investigated in previous model-based studies [7], [9], [10], which is formulated as a set of PDEs consisting of the continuum equation and Eikonal equation, as shown in Equation (16). At the dynamic level, the traditional Lax-Friedriches (LF) method is applied to solve the continuum equation, while at the static level, FSM and NES-DI are applied to solve the Eikonal equation, respectively.

$$\rho_t(x, y, t) + \nabla \cdot \boldsymbol{f}(x, y, t) = 0, \forall (x, y) \in \Omega, \quad t \in T, \quad (16a)$$

$$c(x, y, t) \frac{\boldsymbol{f}(x, y, t)}{\|\boldsymbol{f}(x, y, t)\|} = -\nabla \phi(x, y, t), \ \forall (x, y) \in \Omega, t \in T, \quad (16b)$$

$$\|\nabla \phi(x, y, t)\| = c(x, y, t), \ \forall (x, y) \in \Omega, \ t \in T, \quad (16c)$$

where $\rho_t(x, y, t) = \partial \rho(x, y, t)/\partial t$, $\|\boldsymbol{f}(x, y, t)\|$ denotes the magnitude of the flow rate which is assumed with the fundamental diagram, i.e. $\|\boldsymbol{f}(x, y, t)\| = 1.034\rho \exp(-0.075\rho^2)$, and $c(x, y, t)$ denotes the cost distribution which is

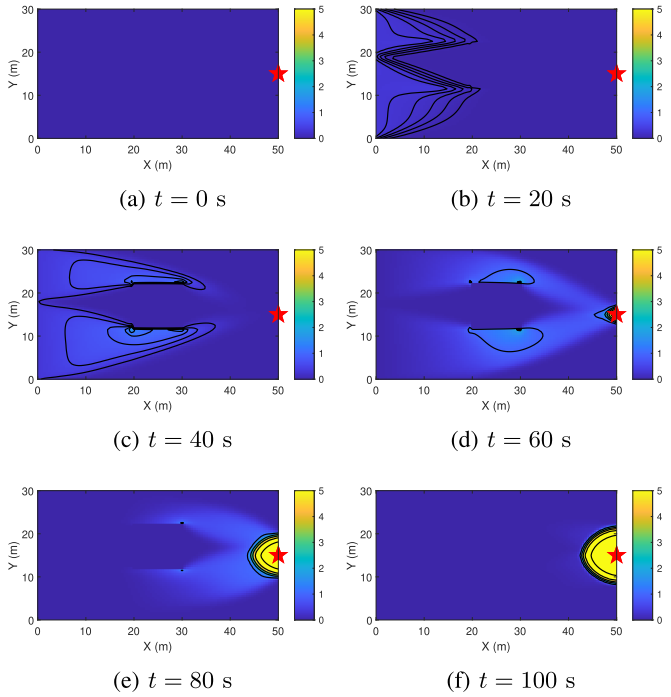

Fig. 8. Distribution of density derived from the dynamic RDUE model for example 3. (Unit: ped/m^2).

determined by

$$c(x, y, t) = \begin{cases} \dfrac{1}{1.034 \exp(-0.075\rho^2)} + 0.005\rho^2, \\ \qquad (x, y) \notin \Gamma_H, \\ 100, \qquad (x, y) \in \Gamma_H. \end{cases} \tag{17}$$

The whole computational domain is $\Omega : [0, 50]$ m $\times [0, 30]$ m. The inflow boundary is located at $\Gamma_O : [0, 0]$ m $\times [0, 30]$ m, and the destination is located at $\Gamma_D : (50, 15)$. The obstacle is located at $\Gamma_H : [20, 30]$ m $\times [8, 18]$ m. The railway platform is initially empty at $t = 0$ s. In the dynamic simulation, pedestrians enter the platform through the inflow boundary and progress from left to right towards their destination on the platform, as depicted in Fig. 8. The traditional numerical methods, including LF and FSM simulate pedestrians. Then, NES-DI is applied dynamically to compute the distribution of cost potential at each time step, with an update interval of 1 second, based on the instantaneous total cost.

Considering the large computational burden of dynamic problem, a comparative analysis was conducted on three distinct algorithms for 100 s, encompassing 101 time steps within a computational domain characterized by a mesh configuration of 101×61, including FSM, NES-DI(I), and NES-DI(I) with transfer learning. Given the absence of an exact analytical solution for the scenario under investigation, the solution derived from the FSM algorithm, utilizing a mesh size of 1001×601, is designated as the ground truth solution for benchmarking purposes. Due to the error accumulation problem, distance information is re-calibrated by FSM when the performance of NES-DI(I) with transfer learning is worse than FSM after several time steps. To better decide the time for re-calibration, the Hamiltonian loss of the free area is introduced as an independent criterion in Eq.(18).

$$L_{free}(\boldsymbol{\theta}, \boldsymbol{\beta}, p) = \frac{1}{N_{free}} \sum_{\mathbf{x}_r \notin \Gamma_H} |\mathcal{H}_p(\mathbf{x}_r, \phi_{\boldsymbol{\theta},\boldsymbol{\beta}})|, \tag{18}$$

where N_{free} is the total number of receiver points in the free area, $\mathbf{x}_r \notin \Gamma_H$ denotes the receiver points in the free area, $\mathcal{H}_p$ is formulated in Eq. (10). After completing the training of the neural networks for each time step, the potential can be predicted given the cost input, and the Hamiltonian loss value of the free area can be calculated accordingly, which is independent of FSM. In addition, the percentage of the exceeding value of the Hamiltonian loss of free area at each time step compared to the time step after re-calibration can also be calculated and used to roughly determine whether re-calibration should be performed, see Eq.(19).

$$E_{t_i} = \frac{|L_{free_{t_i}} - L_{free_{t_0}}|}{L_{free_{t_0}}} \times 100\%, \tag{19}$$

where E_{t_i} denotes the exceeding percentage of Hamiltonian loss of free area at time step t_i, $L_{free_{t_i}}$ is the Hamiltonian loss of free area at time step t_i, and $L_{free_{t_0}}$ is the Hamiltonian loss of free area at time step t_0 after re-calibration. However, there is a trade-off between efficiency and accuracy. Specifically, if the tolerance of this criterion is high, the number of permissible transfer steps would increase, but the error accumulation would be more severe, and vice versa. Therefore, a pre-experiment is recommended to select a suitable value for this criterion in real-world applications.

To elucidate the efficacy of transfer learning within this context, a specific interval from 56 s to 61 s, a period marked by significant alterations, is highlighted. Within this interval, the predicted solution contours of the potential distribution are presented in Fig. 9, and the detailed RMAE and training time are compared in Table IV. RMAE of the whole computational domain that excludes obstacles over time are presented in Fig. 10.

Based on Table IV, it can be found that both NES-DI(I) and NES-DI(I)-transfer outperform FSM in RMAE of all (x, y) and $(x, y) \notin \Gamma_H$ throughout a duration of 6 s. In comparison to FSM, NES-DI stably stachieves RMAE reductions exceeding 12% for all (x, y) and 15% for $(x, y) \notin \Gamma_H$. Notably, NES-DI(I)-transfer demonstrates the best performance in the first several time steps, but gradually get worse than NES-DI(I) and even FSM in later time steps as more transfer steps are implemented. The possible reason is that immediately after calibration, the distance information of NES-DI(I)-transfer is relatively accurate. Although compared to NES-DI(I), NES-DI(I)-transfer has less accurate distance information, it may give the neural networks more freedom during the learning process to explore solutions rather than exploiting the given distance information, and the neural network can even further improve the performance in the learning progress, resulting in an initial decrease in RMAE over time.

However, as time progresses, the continuous accumulation of errors causes the distance information to become increasingly inaccurate, which in turn misleads the neural network,

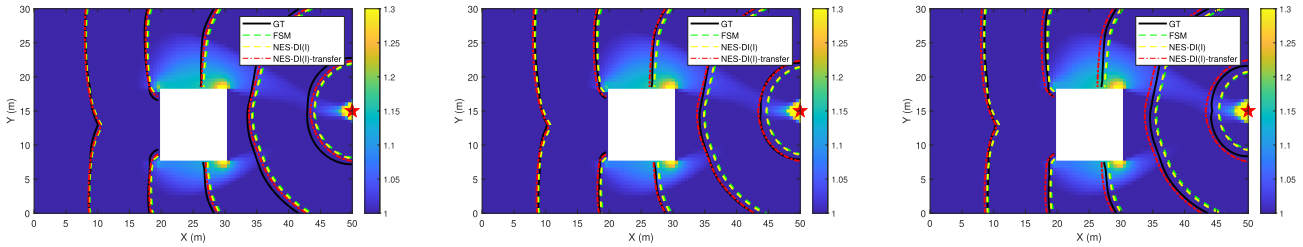

(a) $t = 56$ s (b) $t = 57$ s (c) $t = 58$ s

(d) $t = 59$ s (e) $t = 60$ s (f) $t = 61$ s

Fig. 9. Contours of the potential distribution predicted using FSM, NES-DI(I), and NES-DI(I) with transfer learning in the free area compared to ground truth solution (GT) for example 3. The heatmaps show the cost magnitude in the free area.

TABLE IV
PERFORMANCE COMPARISON OF FSM, NES-DI(I), AND NES-DI(I) WITH TRANSFER LEARNING IN EXAMPLE 3

Solver	Time (s)	RMAE of all (x, y) (%)	RMAE of $(x, y) \notin \Gamma_H$ (%)	Hamiltonian loss of $(x, y) \notin \Gamma_H$	Exceeding percentage (%)	Training time (s) / Epoch number	Inference time (s)
FSM	56	8.17	6.67				
FSM	57	7.64	5.95				
FSM	58	8.05	6.55	–	–	–	–
FSM	59	8.13	6.66				
FSM	60	8.26	6.86				
FSM	61	7.80	6.28				
NES-DI(I)	56	7.19	5.67	0.0364		14.85/ 200	0.05
NES-DI(I)	57	6.74	5.00	0.0365		14.91/ 200	0.05
NES-DI(I)	58	7.04	5.51	0.0367	–	14.50/ 200	0.05
NES-DI(I)	59	7.03	5.54	0.0371		14.77/ 200	0.05
NES-DI(I)	60	7.07	**5.65**	0.0372		14.87/ 200	0.05
NES-DI(I)	61	**6.33**	**4.80**	0.0375		14.93/ 200	0.05
NES-DI(I)-transfer	56	**5.64**	**3.56**	0.0370	0	14.63/ 200	0.05
NES-DI(I)-transfer	57	**3.36**	**0.47**	0.0385	4.05	14.65/ 200	0.05
NES-DI(I)-transfer	58	**4.10**	**1.95**	0.0404	9.19	14.94/ 200	0.05
NES-DI(I)-transfer	59	**5.34**	**4.18**	0.0428	10.53	14.50/ 200	0.05
NES-DI(I)-transfer	60	**6.53**	6.23	0.0449	21.35	14.82/ 200	0.05
NES-DI(I)-transfer	61	8.07	8.76	0.0469	26.76	14.73/ 200	0.05

leading to a gradual increase in RMAE over time. Furthermore, since the loss from the obstacle area has a significant impact on the overall loss function, NES-DI(I)-transfer tends to focus on learning to solve the potential in the obstacle area during training. Nevertheless, due to the strong cost disparity between the obstacle area and the free area, NES-DI(I)-transfer struggles to effectively learn to solve the potential in the free area, resulting in deteriorating performance in that region.

Since the potential of the obstacle area greatly influences the global RMAE calculation, the results show that the overall RMAE of NES-DI(I)-transfer is mostly lower than that of NES-DI(I). However, regarding the RMAE of $(x, y) \notin \Gamma_H$, the performance of NES-DI(I)-transfer is often worse than that of NES-DI(I), with RMAE increasing as the number of transfer steps increases. This trend persists to the point where the RMAE of NES-DI(I)-transfer surpasses that of FSM, necessitating the deployment of NES-DI(I) for re-calibrating the distance information to rectify this discrepancy. Besides, based on the exceeding percentage of Hamiltonian loss of the free area, the threshold for re-calibration can be set to around 25% in this case. Note that there is no absolute threshold for this criterion, it depends on the trade-off between efficiency and accuracy.

Fig. 9 facilitates an intuitive understanding of the temporal evolution of solution contours, highlighting a divergence in the solution contours generated by NES-DI(I)-transfer from those produced by FSM and NES-DI(I). This divergence underscores the issue of error accumulation attributable to inaccuracies in distance information as time progresses. Further analysis of the overall evacuation process performance, as depicted

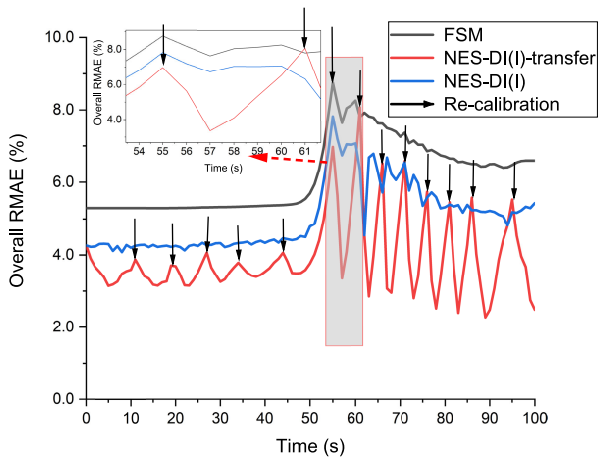

(a) RMAE of all (x, y) (%)

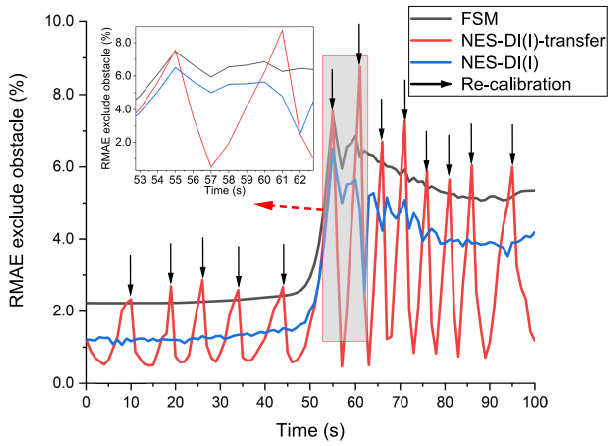

(b) RMAE of $(x, y) \notin \Gamma_H$ (%)

Fig. 10. RMAE overtime of FSM, NES-DI(I), and NES-DI(I)-transfer in the whole computational domain and free area in example 3.

in Fig. 10, corroborates that NES-DI(I)-transfer consistently outperforms its counterparts in minimizing RMAE across all (x, y). Nonetheless, there is a gradual accrual of error in the RMAE concerning $(x, y) \notin \Gamma_H$. To mitigate this, recalibration interventions are executed on nine occasions throughout the total span of 100 s, ensuring that NES-DI(I)-transfer maintains its superior performance in RMAE of $(x, y) \notin \Gamma_H$. This strategic recalibration underscores the necessity of continuous monitoring and adjustment to harness the full potential of NES-DI(I)-transfer, particularly in dynamic computational environments.

In terms of efficiency, NES-DI(I) and NES-DI(I)-transfer show similar training time and inference time. However, NES-DI(I)-transfer saves the computational time of the numerical method compared to NES-DI(I) by transferring the solution of the previous time step as distance information. As the mesh sizes become denser, more computational time is saved, the computational times of FSM for the potential filed at time $t = 60$ s under different mesh sizes are shown in Fig. 11 (performed on CPU Intel Core i9-12900KF).

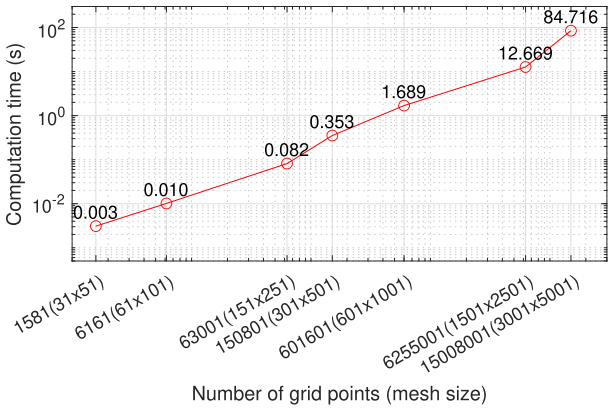

Fig. 11. Computational times of FSM with respect to mesh size for example 3.

Nonetheless, it is critical to acknowledge that, despite these improvements, the computational efficiency of the NES-DI(I)-transfer remains markedly inferior when evaluated against the benchmarks set by traditional numerical methods. This disparity underscores the necessity for future research and development in NES-DI algorithms to narrow the efficiency chasm with established numerical methodologies, enhancing their applicability and performance in dynamic problem-solving contexts.

VI. Discussion

A. Comparison of NES-DI and Other Methods

Unlike other problems described by the Eikonal equation, obstacles with extremely high costs are very common in macroscopic continuum traffic flow models, which introduce the strong heterogeneity and singularity issues in solving the RDUE problem.

Upon analyzing the outcomes derived from three distinct scenarios involving Eikonal equations, it is evident that the NES-DI approach confers several advantages over conventional numerical methods (e.g., FSM). Initially, the NES-DI algorithm demonstrates enhanced performance in resolving the RDUE problem characterized by a strong heterogeneous cost field, compared to the traditional first-order FSM. Remarkably, in the RDUE problem that predicts the route choices in urban areas under the mesh size of 1001×1001, the algorithm's performance has been improved by over 51%, circumventing the need for an increased density of grid points.

Furthermore, unlike traditional numerical techniques limited to calculating potential at predetermined grid points, NES-DI boosts the capability to predict potential at any given location within the computational domain. Additionally, NES-DI, as a mesh-free methodology, exhibits the ability to accommodate arbitrary cost field configurations, thereby offering considerable flexibility for real-world DTA implementations. In contrast, conventional numerical methods mandate the specification of the cost field in a mesh grid format.

Finally, although some high-order numerical methods can outperform the first-order numerical method, they suffer from ghost-point issues: Updating the potential at a specific point necessitates a broad stencil. This requirement is problematic

at the domain boundaries, where there are insufficient points within the stencils. Here, extrapolation methods are required to approximate these "ghost points". While there have been extensive discussions on the most appropriate extrapolation methods, the problem persists in influencing the convergence of Gaussian-Seidel iterations [11]. Through incorporating PINNs, NES-DI bypasses this issue present in higher-order FSM.

Compared to other PINNs methods (e.g., NES), the NES-DI framework exhibits substantial superiority in addressing RDUE problems characterized by strong heterogeneity. First, addressing the inaccuracy of distance information inherent to NES, NES-DI ingeniously incorporates the DI module by factorizing Eikonal equation. This module leverages numerical methods to provide precise initial distance information, significantly improving predictive performance. Specifically, in the RDUE problem that predicts the route choices in urban areas under the mesh size of 1001×1001, NES-DI reduces RMAE by over 85% compared to NES.

Furthermore, this approach effectively harnesses the strengths of numerical solutions in highly heterogeneous cost fields, substantially alleviating the computational burden on PINNs when solving Eikonal equation of problems with strong heterogeneity. Notably, NES-DI only requires far fewer training epochs than NES to achieve good performance, demonstrating an improvement in computational efficiency of over 90%.

Additionally, as the size of training data increases, the performance of NES-DI is significantly improved, whereas the performance of NES remains poor and is barely improved. Consequently, in practical applications, NES-DI can benefit from performance gains by acquiring more training data when addressing problems with strong heterogeneity.

Besides, given the extensive application of the Eikonal equation across diverse domains such as optics, seismology, and video-game rendering, it is anticipated that NES-DI could be aptly applicable in these fields. Particularly, it could be highly beneficial in scenarios that involve Eikonal equation coupled with strong heterogeneity.

B. The Influence of Distance Information

One of the most significant contributions of this study is identifying the importance of distance information. By providing an accurate distance matrix, NES-DI can handle strong heterogeneous problems well. Moreover, by comparing experiment results between NES-DI and NES-DI(I), it can be found that introducing MAKIMA interpolation to densify the distance matrix can significantly boost algorithmic performance in scenarios with sparse mesh sizes of data points. This is because the accuracy of this approximation hinges on the inference derived from F_θ and the distance estimation from R_β, as depicted in the inference framework in Fig. 2. When a larger grid size is used, the FSM yields more accurate distance information of $\mathbf{R}^{M\times N}$, leading to a more precise distance estimation. As a result, the performance of NES-DI improves. Nonetheless, MAKIMA interpolation may become redundant, potentially engendering interpolation inaccuracies that could mislead PINNs and consequently degrade the model's accuracy. Therefore, it is prudent to meticulously select the most suitable algorithm, considering the size of training data available in specific practical scenarios. This strategic selection ensures the alignment of the algorithm's capabilities with the nuanced requirements of the data landscape, thereby optimizing the computational model's efficacy in tackling the complexities of heterogeneous problems.

Moreover, in exploring RDUE problems at the dynamic level, error accumulation emerges as a significant challenge, primarily attributed to inaccuracies in distance information propagated from preceding time steps. These inaccuracies have the potential to constrict and mislead neural networks, thereby obstructing their capacity to discern the genuine solution. Consequently, developing methodologies that provide accurate initial distance information emerges as a research avenue of substantial merit, warranting thorough investigation.

C. Limitations and Future Studies

It is worth noting that traditional numerical methods have evolved for several decades to be successfully applied in many applications. Although this study proposes a powerful NES-DI framework that shows great potential in solving the RDUE problem, it has several limitations and needs further improvements. First, although NES-DI outperforms numerical methods in solving RDUE problems and has demonstrated significant improvement in training time compared to other PINNs methods, the efficiency of NES-DI is worse than that of numerical methods. Second, when solving the RDUE problem at the dynamic level, the transfer framework of NES-DI faces the error accumulation issue due to inaccurate distance information, since utilizing the solution of the previous time step as distance information might mislead PINNs in solving RDUE at a new time step, especially when the cost field has greatly changed. Future studies could explore potentially more efficient model structures or training techniques to reduce the training time of neural networks. Efforts should also be made to solve the RDUE problem at the dynamic level more efficiently and accurately using PINN-based methods.

VII. Conclusion

In this study, we proposed a PINNs-based framework, i.e., NES-DI, to solve the Eikonal equation in RDUE model for macroscopic continuum traffic flow. To overcome the limitation of traditional NES, we take advantage of factorized Eikonal equation and integrate a simple numerical method to provide accurate distance information. The proposed framework combined the advantage of the numerical method in dealing with strong heterogeneity and the advantage of PINNs in accuracy and flexibility, which is mesh-free and can predict the traffic states at arbitrary locations within the continuum space. Numerical examples, including trigonometric Eikonal equation with analytical solutions, RDUE problem that predicts route choices in urban areas, and RDUE problem that dynamically predicts pedestrian route choices for railway platform evacuation, are conducted to testify the effectiveness of the proposed NES-DI framework. The success of NES-DI in

solving RDUE problems has validated the efficacy of employing the PINNs approach in solving PDEs in macroscopic traffic flow studies, which provides novel perspectives and directions for future research on PDE-related models in transportation studies.

REFERENCES

[1] J. Du, S. C. Wong, C.-W. Shu, T. Xiong, M. Zhang, and K. Choi, "Revisiting Jiang's dynamic continuum model for urban cities," *Transp. Res. B, Methodol.*, vol. 56, pp. 96–119, Oct. 2013.

[2] Y.-Q. Jiang, W. Zhang, and S.-G. Zhou, "Comparison study of the reactive and predictive dynamic models for pedestrian flow," *Phys. A, Stat. Mech. Appl.*, vol. 441, pp. 51–61, Jan. 2016.

[3] R. Aghamohammadi and J. A. Laval, "Dynamic traffic assignment using the macroscopic fundamental diagram: A review of vehicular and pedestrian flow models," *Transp. Res. B, Methodol.*, vol. 137, pp. 99–118, Jul. 2020.

[4] C. Wu, L. Yang, J. Du, X. Pei, and S. C. Wong, "Continuum dynamic traffic models with novel local route-choice strategies for urban cities," *Transp. Res. B, Methodol.*, vol. 181, Mar. 2024, Art. no. 102888.

[5] R. L. Hughes, "A continuum theory for the flow of pedestrians," *Transp. Res. B, Methodol.*, vol. 36, no. 6, pp. 507–535, 2002.

[6] R. Zhao, Q. Hu, Q. Liu, C. Li, D. Dong, and Y. Ma, "Panic propagation dynamics of high-density crowd based on information entropy and aw-rascle model," *IEEE Trans. Intell. Transp. Syst.*, vol. 21, no. 10, pp. 4425–4434, Oct. 2020.

[7] H. Liang, J. Du, and S. C. Wong, "A continuum model for pedestrian flow with explicit consideration of crowd force and panic effects," *Transp. Res. B, Methodol.*, vol. 149, pp. 100–117, Jul. 2021.

[8] Y. Jiang, S. C. Wong, H. W. Ho, P. Zhang, R. Liu, and A. Sumalee, "A dynamic traffic assignment model for a continuum transportation system," *Transp. Res. B, Methodol.*, vol. 45, no. 2, pp. 343–363, Feb. 2011.

[9] L. Yang, H. Liang, J. Du, and S. C. Wong, "Positivity-preserving discontinuous Galerkin methods on triangular meshes for macroscopic pedestrian flow models," *J. Adv. Transp.*, vol. 2023, pp. 1–19, Oct. 2023.

[10] L. Huang, S. C. Wong, M. Zhang, C.-W. Shu, and W. H. K. Lam, "Revisiting Hughes' dynamic continuum model for pedestrian flow and the development of an efficient solution algorithm," *Transp. Res. B, Methodol.*, vol. 43, no. 1, pp. 127–141, Jan. 2009.

[11] T. Xiong, M. Zhang, C.-W. Shu, S. C. Wong, and P. Zhang, "High-order computational scheme for a dynamic continuum model for bi-directional pedestrian flows," *Comput.-Aided Civil Infrastruct. Eng.*, vol. 26, no. 4, pp. 298–310, May 2011.

[12] L. L. Tatarinova and M. E. Garcia, "Exact solutions of the Eikonal equations describing self-focusing in highly nonlinear geometrical optics," *Phys. Rev. A, Gen. Phys.*, vol. 78, no. 2, Aug. 2008, Art. no. 021806.

[13] X. Desquesnes, A. Elmoataz, O. Lézoray, and V. Ta, "Efficient algorithms for image and high dimensional data processing using Eikonal equation on graphs," in *Proc. ISVC*. Cham, Switzerland: Springer, Jan. 2010, pp. 647–658.

[14] A. R. Bruss, "The Eikonal equation: Some results applicable to computer vision," *J. Math. Phys.*, vol. 23, no. 5, pp. 890–896, May 1982.

[15] Y. Liu and P. Tong, "Eikonal equation-based P-wave seismic azimuthal anisotropy tomography of the crustal structure beneath northern California," *Geophys. J. Int.*, vol. 226, no. 1, pp. 287–301, Mar. 2021.

[16] Y.-T. Zhang, H.-K. Zhao, and J. Qian, "High order fast sweeping methods for static Hamilton–Jacobi equations," *J. Sci. Comput.*, vol. 29, no. 1, pp. 25–56, Oct. 2006.

[17] J. A. Sethian, "Fast marching methods," *SIAM Rev.*, vol. 41, no. 2, pp. 199–235, Jan. 1999.

[18] J. Qian, Y.-T. Zhang, and H.-K. Zhao, "Fast sweeping methods for Eikonal equations on triangular meshes," *SIAM J. Numer. Anal.*, vol. 45, no. 1, pp. 83–107, Jan. 2007.

[19] Y. Xia, S. C. Wong, M. Zhang, C.-W. Shu, and W. H. K. Lam, "An efficient discontinuous Galerkin method on triangular meshes for a pedestrian flow model," *Int. J. Numer. Methods Eng.*, vol. 76, no. 3, pp. 337–350, Oct. 2008.

[20] T. Xiong, M. Zhang, Y.-T. Zhang, and C.-W. Shu, "Fast sweeping fifth order WENO scheme for static Hamilton–Jacobi equations with accurate boundary treatment," *J. Sci. Comput.*, vol. 45, nos. 1–3, pp. 514–536, Oct. 2010.

[21] M. Raissi, P. Perdikaris, and G. E. Karniadakis, "Physics-informed neural networks: A deep learning framework for solving forward and inverse problems involving nonlinear partial differential equations," *J. Comput. Phys.*, vol. 378, pp. 686–707, Feb. 2019.

[22] G. E. Karniadakis, I. G. Kevrekidis, L. Lu, P. Perdikaris, S. Wang, and L. Yang, "Physics-informed machine learning," *Nature Rev. Phys.*, vol. 3, no. 6, pp. 422–440, May 2021.

[23] X. Jin, S. Cai, H. Li, and G. E. Karniadakis, "NSFnets (Navier–Stokes flow nets): Physics-informed neural networks for the incompressible Navier–Stokes equations," *J. Comput. Phys.*, vol. 426, Feb. 2021, Art. no. 109951.

[24] S. Alkhadhr and M. Almekkawy, "A combination of deep neural networks and physics to solve the inverse problem of Burger's equation," in *Proc. 43rd Annu. Int. Conf. IEEE Eng. Med. Biol. Soc. (EMBC)*, Nov. 2021, pp. 4465–4468.

[25] Y. Wang and L. Zhong, "NAS-PINN: Neural architecture search-guided physics-informed neural network for solving PDEs," *J. Comput. Phys.*, vol. 496, Jan. 2024, Art. no. 112603.

[26] U. B. Waheed, E. Haghighat, T. Alkhalifah, C. Song, and Q. Hao, "PINNeik: Eikonal solution using physics-informed neural networks," *Comput. Geosci.*, vol. 155, Oct. 2021, Art. no. 104833.

[27] J. D. Smith, K. Azizzadenesheli, and Z. E. Ross, "EikoNet: Solving the Eikonal equation with deep neural networks," *IEEE Trans. Geosci. Remote Sens.*, vol. 59, no. 12, pp. 10685–10696, Dec. 2021.

[28] S. Grubas, A. Duchkov, and G. Loginov, "Neural Eikonal solver: Improving accuracy of physics-informed neural networks for solving Eikonal equation in case of caustics," *J. Comput. Phys.*, vol. 474, Feb. 2023, Art. no. 111789.

[29] T.-Q. Tang, J.-G. Li, S.-C. Yang, and H.-Y. Shang, "Effects of on-ramp on the fuel consumption of the vehicles on the main road under car-following model," *Phys. A, Stat. Mech. Appl.*, vol. 419, pp. 293–300, Feb. 2015.

[30] T.-Q. Tang, Z.-Y. Yi, and Q.-F. Lin, "Effects of signal light on the fuel consumption and emissions under car-following model," *Phys. A, Stat. Mech. Appl.*, vol. 469, pp. 200–205, Mar. 2017.

[31] C. F. Daganzo, "In traffic flow, cellular automata=kinematic waves," *Transp. Res. B, Methodol.*, vol. 40, no. 5, pp. 396–403, Jun. 2006.

[32] H. Zhang, J. Wei, X. Gao, and J. Hu, "The study of traffic flow model based on cellular automata and naive Bayes," *Int. J. Mod. Phys. C*, vol. 30, no. 5, May 2019, Art. no. 1950034.

[33] W. Wong and S. C. Wong, "Systematic bias in transport model calibration arising from the variability of linear data projection," *Transp. Res. B, Methodol.*, vol. 75, pp. 1–18, May 2015.

[34] Y. Jiang, Z. Ding, J. Zhou, P. Wu, and B. Chen, "Estimation of traffic emissions in a polycentric urban city based on a macroscopic approach," *Phys. A, Stat. Mech. Appl.*, vol. 602, Sep. 2022, Art. no. 127391.

[35] Y. Z. Tao et al., "Dynamic system-optimal traffic assignment for a city using the continuum modeling approach," *J. Adv. Transp.*, vol. 48, no. 7, pp. 782–797, Nov. 2014.

[36] J. Du, S. C. Wong, C.-W. Shu, and M. Zhang, "Reformulating the Hoogendoorn–Bovy predictive dynamic user-optimal model in continuum space with anisotropic condition," *Transp. Res. B, Methodol.*, vol. 79, pp. 189–217, Sep. 2015.

[37] Y.-Q. Jiang, S. C. Wong, P. Zhang, and K. Choi, "Dynamic continuum model with elastic demand for a polycentric urban city," *Transp. Sci.*, vol. 51, no. 3, pp. 931–945, Aug. 2017.

[38] R. L. Hughes, "The flow of large crowds of pedestrians," *Math. Comput. Simul.*, vol. 53, nos. 4–6, pp. 367–370, Oct. 2000.

[39] L. Huang, Y. Xia, S. C. Wong, C.-W. Shu, M. Zhang, and W. H. K. Lam, "Dynamic continuum model for bi-directional pedestrian flows," *Proc. Inst. Civil Eng.-Eng. Comput. Mech.*, vol. 162, no. 2, pp. 67–75, Jun. 2009.

[40] Y. Jiang et al., "A reactive dynamic continuum user equilibrium model for bi-directional pedestrian flows," *Acta Mathematica Scientia*, vol. 29, no. 6, pp. 1541–1555, Nov. 2009.

[41] A. J. Huang and S. Agarwal, "Physics informed deep learning for traffic state estimation," in *Proc. IEEE 23rd Int. Conf. Intell. Transp. Syst. (ITSC)*, Apr. 2020, pp. 1–6.

[42] R. Shi, Z. Mo, and X. Di, "Physics-informed deep learning for traffic state estimation: A hybrid paradigm informed by second-order traffic models," in *Proc. AAAI Conf. Artif. Intell.*, vol. 35, 2021, pp. 540–547.

[43] R. Shi, Z. Mo, K. Huang, X. Di, and Q. Du, "A physics-informed deep learning paradigm for traffic state and fundamental diagram estimation," *IEEE Trans. Intell. Transp. Syst.*, vol. 23, no. 8, pp. 11688–11698, Aug. 2022.

[44] A. J. Huang and S. Agarwal, "Physics-informed deep learning for traffic state estimation: Illustrations with LWR and CTM models," *IEEE Open J. Intell. Transp. Syst.*, vol. 3, pp. 503–518, 2022.
[45] J. Lu, C. Li, X. B. Wu, and X. S. Zhou, "Physics-informed neural networks for integrated traffic state and queue profile estimation: A differentiable programming approach on layered computational graphs," *Transp. Res. C, Emerg. Technol.*, vol. 153, Aug. 2023, Art. no. 104224.
[46] J. Zhang, S. Mao, L. Yang, W. Ma, S. Li, and Z. Gao, "Physics-informed deep learning for traffic state estimation based on the traffic flow model and computational graph method," *Inf. Fusion*, vol. 101, Jan. 2024, Art. no. 101971.
[47] C. Zhao and H. Yu, "Observer-informed deep learning for traffic state estimation with boundary sensing," *IEEE Trans. Intell. Transp. Syst.*, vol. 25, no. 2, pp. 1602–1611, Feb. 2024.
[48] Z. Mo, R. Shi, and X. Di, "A physics-informed deep learning paradigm for car-following models," *Transp. Res. C, Emerg. Technol.*, vol. 130, Sep. 2021, Art. no. 103240.
[49] J. Liu, R. Jiang, J. Zhao, and W. Shen, "A quantile-regression physics-informed deep learning for car-following model," *Transp. Res. C, Emerg. Technol.*, vol. 154, Sep. 2023, Art. no. 104275.
[50] M. Geng, J. Li, Y. Xia, and X. Chen, "A physics-informed transformer model for vehicle trajectory prediction on highways," *Transp. Res. C, Emerg. Technol.*, vol. 154, Sep. 2023, Art. no. 104272.
[51] K. He, X. Zhang, S. Ren, and J. Sun, "Delving deep into rectifiers: Surpassing human-level performance on imagenet classification," in *Proc. IEEE Int. Conf. Comput. Vis. (ICCV)*, Dec. 2015, pp. 1026–1034.
[52] Y. Jiang, B. Chen, X. Li, and Z. Ding, "Dynamic navigation field in the social force model for pedestrian evacuation," *Appl. Math. Model.*, vol. 80, pp. 815–826, Apr. 2020.
[53] MathWorks. (Apr. 2019). *Makima Piecewise Cubic Interpolation*. [Online]. Available: https://blogs.mathworks.com/cleve/2019/04/29/
[54] S. J. Reddi, S. Kale, and S. Kumar, "On the convergence of Adam and beyond," 2019, *arXiv:1904.09237*.
[55] R. Pan, F. Xiao, and M. Shen, "Ro-PINN: A reduced order physics-informed neural network for solving the macroscopic model of pedestrian flows," *Transp. Res. C, Emerg. Technol.*, vol. 163, Jun. 2024, Art. no. 104658.

Yun Ye (Member, IEEE) received the B.E. degree from the Department of Civil Engineering, Zhejiang University, in 2017, and the Ph.D. degree from The University of Hong Kong, in 2021. He is currently an Associate Professor with Ningbo University. His research interests include virtual reality, intelligent transportation systems, pedestrian-vehicle interaction, traffic safety, and human factors.

Haoyang Liang (Member, IEEE) received the B.S. degree from the Department of Civil Engineering, Tsinghua University, in 2018, and the Ph.D. degree from The University of Hong Kong, in 2022. He is currently a Post-Doctoral Researcher with Tongji University, where he is also the Principal Investigator of TransCAVE Laboratory, focusing on developing digital twin platforms for mixed traffic simulation and testing. His research interests include crowd dynamics, pedestrian-vehicle interaction, virtual reality, and human factors.

Jian Sun (Member, IEEE) received the Ph.D. degree from Tongji University in 2006. Subsequently, he was with Tongji University as a Lecturer and then promoted to the position as a Professor in 2011, where he is currently a Professor with the College of Transportation Engineering and the Dean of the Department of Traffic Engineering. His main research interests include traffic flow theory, traffic simulation, connected vehicle-infrastructure systems, and intelligent transportation systems.

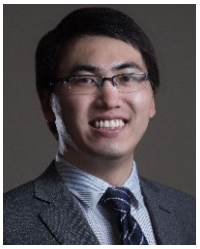

Xiqun (Michael) Chen received the B.E. and Ph.D. degrees from the Department of Civil Engineering, Tsinghua University, China, in 2008 and 2013, respectively. He is currently a Tenured Professor with Zhejiang University and the Director of the Institute of Intelligent Transportation Systems. His research interests include intelligent transportation systems, shared mobility on demand, simulation-based optimization, and transportation big data analytics. He received the 2013 IEEE Intelligent Transportation Systems Society Best Ph.D. Dissertation Award and has published one book, three book chapters, over 150 peer-reviewed journal articles, and over 100 conference papers. He serves as the Chair for Transportation Management and Mobility Service of World Transport Convention, an Associate Editor of *Transportation Research Part C: Emerging Technologies*, an Associate Editor of IEEE TRANSACTIONS ON INTELLIGENT VEHICLES, and Editorial Advisory Board Member of *npj Sustainable Mobility and Transport*.